Hindawi
Geofluids
Volume 2022, Article ID 6792154, 13 pages
https://doi.org/10.1155/2022/6792154

Research Article

Experimental Investigation of Seepage Mechanism on Oil-Water Two-Phase Displacement in Fractured Tight Reservoir

Xuyang Zhang,[1] Jianming Zhang,[1] and Cong Xiao [2,3]

[1]*Baikouquan Oil Production Plant, PetroChina Xinjiang Oilfield Company, China*
[2]*Key Laboratory of Petroleum Engineering, Ministry of Education, China University of Petroleum, Beijing 102249, China*
[3]*College of Petroleum Engineering, China University of Petroleum, Beijing 102249, China*

Correspondence should be addressed to Cong Xiao; c.xiao@tudelft.nl

Received 17 July 2021; Revised 23 September 2021; Accepted 5 November 2021; Published 10 January 2022

Academic Editor: Bailu Teng

As a type of unconventional oil and gas resources, tight sandstone reservoir has low permeability and porosity properties and thus is commonly necessary to develop through hydraulic fracturing treatment. Due to the coexistence of natural fractures and induced hydraulic fractures, the heterogeneity of reservoir permeability becomes severe and therefore results in complicated fluid seepage mechanism. It is of significance to investigate the oil-water two-phase seepage mechanics before and after the hydraulic fracturing stimulation with the aim of supporting the actual production and development of oilfield. This paper experimentally investigated the influences of fracture system on seepage characteristics of two-phase displacement in sample cores of fractured tight sandstones. In details, the changes of injection rate, cumulative production rate, recovery ratio, and water content were analyzed before and after the hydraulic fracturing treatments. To further analyze the displacement characteristics of the sample core, the displacement indices of four rock samples in different displacement stages were investigated. The sensitivity of sample core displacement indices to many key factors, including injection time, oil production rate, oil recovery factor and injection multiple factor, and moisture (i.e., water content was 95%, 98%, and 99.5%, respectively), before and after the hydraulic fracturing treatments were obtained synthetically. Besides, the relationship between recovery difference and contribution of fracture to permeability was explored at different water contents. The experimental results reveal that the fracture system shortens the water-free production period and hence reduces the recovery rate. The greater the contribution of fractures to permeability, the lower the recovery of water during this period.

1. Introduction

With the increase of the energy demand, unconventional oil and gas resources have gained more attention and popularity around the world; among them, the tight sandstone reservoir is one of the most important unconventional oil and gas resources. Since tight sandstone reservoirs generally have low porosity and low permeability properties, hydraulic fracturing treatment has become one of the most feasible and dispensable methods to effectively and economically develop the oil and gas resources from the tight reservoir. The high-conductive fracture systems induced by the hydraulic fracturing stimulation have a great influence on oil-sweeping efficiency, cap-rock integrity, well injectivity, and water breakthrough [1–3]. The study on the fracturing treatments, fracture types, fracture seepage mechanism, and orientation of the well placement will contribute to the development of tight reservoirs, which can enhance the oil production rate and the final recovery [4–6].

After hydraulic fracturing treatment in the tight reservoir, both the preexisting natural fractures in the reservoir and the hydraulic fractures induced by fracturing treatment increase the permeability heterogeneity of tight sandstone reservoir, resulting in highly complicated oil-water distribution. This has a great influence on the two-phase seepage mechanism in the fractured porous media [7]. Due to the strong permeability heterogeneity, it is often difficult to establish an explicit model to characterize the fluid seepage in the fractured reservoirs. To characterize the permeability heterogeneity of tight sandstone, Warren and Root [8],

Kazemi [9], and De Swaan [10] simplified the fracture reservoir into a dual-porosity model through introducing matrix and fracture system, which can be used to provide storage and flow space, respectively. Yu [11] used fractal dimension to construct an analytical model which is expressed as a function of porosity and pore scale. Moinfar et al. [12] developed an efficient embedded discrete fracture model to simulate the flow in fractured reservoirs. Matei et al. [13] recently proposed a projection-based embedded discrete fracture model to simulate the flow in fractured reservoir with highly complex fracture system.

Fully understanding of the two-phase seepage mechanism in porous media is of great importance to effectively develop the tight reservoirs. The permeability capacity due to the existence of fractures is a key parameter to describe the characteristics of the fluid flow behavior. Therefore, it is very important to derive the relative permeability through considering the effects of fractures, which significantly prompts the waterflooding process of fractured reservoirs. In recent years, Yu and Li [14] deduced an analytical equation of relative permeability by use of capillary bundle model [14–19]. Based on Yu's model, Liu et al. [1] took the effect of capillary pressure into consideration and derived a more comprehensive relative permeability model [1, 11]. Lian et al. [20] experimentally investigated the oil-water relative permeability of carbonate cores from the carbonate reservoir and compared differences in the relative permeability curve between natural matrix cores and artificial fracturing cores. Rasmussen [21] conducted a set of laboratory characterization of fluid flow parameters in a porous rock containing a discrete fracture. The sensitivity of various parameters to fluid seepage behavior was analyzed. Joonaki and Ghanaatian [22] derived a predictive model of relative permeability for multiphase flow in fractured oil reservoirs by the use of a soft computing approach. Although aforementioned literature has conducted a study on the calculation of relative permeability for fractured reservoirs, neither of them considered the effect of immobile wettability and nonwetting phase saturation.

The two-phase seepage mechanism in fractured porous media is of great importance to the development of fractured reservoirs, and the relative permeability is a key parameter to describe the characteristics of two-phase seepage process. Leverett [23] applied the steady-state method and conducted the oil-water two-phase experiment through the sand-filling model. It was found that the pressure measurement error at the core end was large due to the capillary discontinuity at the low flow rate. The relative permeability is related to pore throat distribution, pressure gradient, and displacement velocity. In order to eliminate the influence of the core "end effect" in the steady-state method, Rapoport and Leas [24] added a semipermeable baffle to the upper and lower reaches of the core to conduct the gas displacement experiment, so as to better avoid the influence of the end effect on the seepage resistance in the lower reaches of the core. Maldal et al. [25] showed that the relative permeability measured by the steady-state method cannot well simulate the oil-water seepage and saturation distribution under the actual formation conditions. Buckley and Leverett [26] derived the isosaturation plane movement equation of unsaturated seepage by assuming that fluid is incompressible and water content is only a function of water saturation and ignoring capillary pressure, combined with the law of conservation of mass. Welge [27] studied the recovery of gas flooding based on the Buckley-Leverett equation and calculated the relative permeability through the material balance equation and Darcy formula. Schembre and Kovscek [28] studied the relative permeability curve through spontaneous inhalation experiments, during which they used CT scans to calculate the water saturation profile. Bryant and Blunt [29] developed a close-packed sphere model and calculated the relative permeability curve using the close-packed sphere model.

To provide laboratory analysis results for characterizing the seepage mechanism through the fractured porous media and thus supporting the production and development of tight sandstone reservoirs, the true-axial stress equipment is used to form artificial fractures in the scale of core sample. And then the oil-water two-phase displacement experiment was carried out on the core sample before and after the hydraulic fracturing treatment, respectively. Besides, the impact of the fractures on oil recovery varies at different production stages [30]. The changes of injection rate, cumulative production rate, recovery ratio, and water content were analyzed before and after the hydraulic fracturing treatment. To further investigate the displacement characteristics of the sample core, the displacement indices of four rock samples in different displacement stages were analyzed. The sensitivity of core displacement indices to many key factors, including injection time, oil production rate, oil recovery factor and injection multiple factor, and moisture (i.e., water content was 95%, 98%, and 99.5%, respectively), before and after construction of the fracture were obtained synthetically. Three experimental metrics, including the water breakthrough time, water content, and the oil recovery, were used to quantitatively analyze the experimental results.

The remainder of this work is structured as follows: The experiment settings, including geological model description and experiment samples, are provided in Section 2. Section 3 describes the experiment methods and procedure for the two-phase flooding process. Section 4 provides the experimental results and analysis. Section 5 points our some valuable discussion based on the experimental results. Finally, Section 6 summarizes our contribution and points out some potential extensions.

2. Geological Model Description and Experiment Settings

In this work, our research objective is Chang 7 tight sandstone reservoir in Heshui, Longdong reservoir formation in Ordos basin. Chang 7 reservoir has poor physical property with abundant fractures. Through the observation of cores combined with identification of core section and analysis of electron microscope, it is found that macroscopic and microscopic fractures in Chang 7 area are well developed in both sandstone and mudstone, as has been shown in Figure 1. The fractures are dominated by high-angle near-

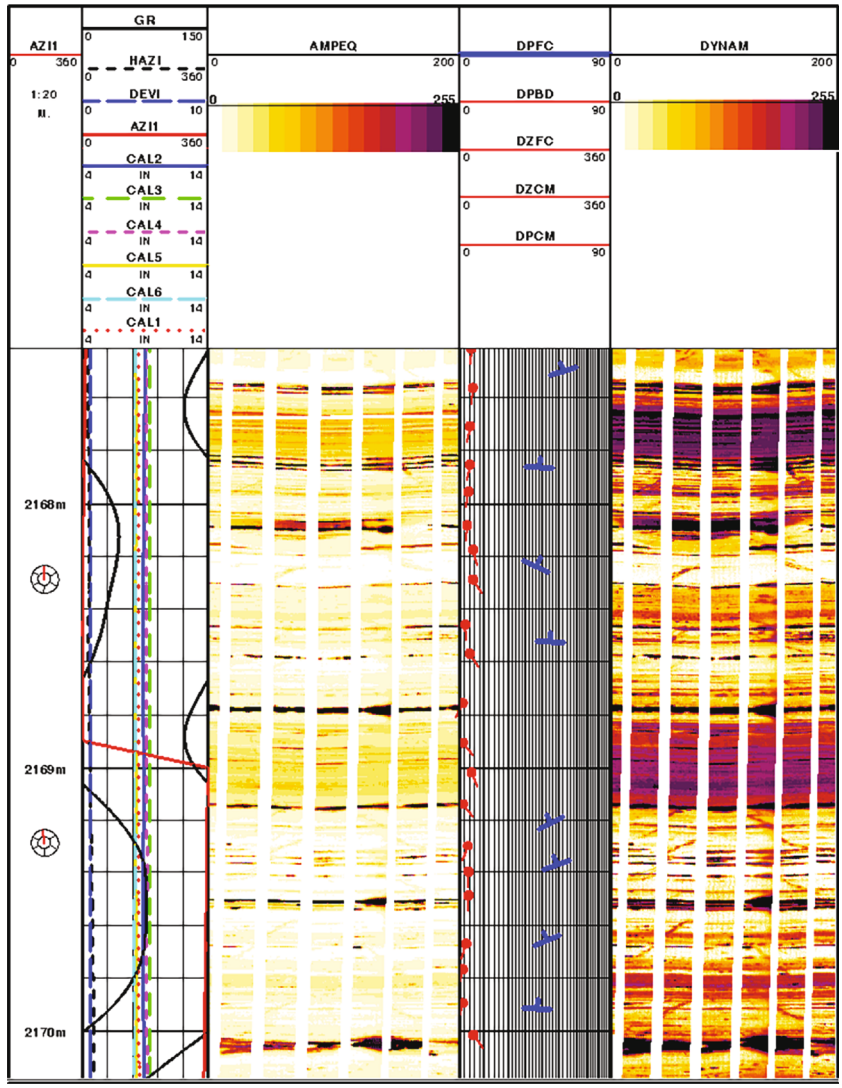

Figure 1: The cracks of well 124 in Chang 7 area. The distribution of fracture can be measured by imaging and well logging technology.

vertical fractures, and the fracture surfaces are mostly flat, which are shear gaps formed by tectonic action.

Both Figures 2 and 3 are schematic diagrams of a two-phase displacement experimental apparatus. A high-pressure, high-speed syringe pump (i.e., Quizix pump) is connected to two high-pressure vessels containing experimental oil and experimental water. This syringe pump provides the required displacement power in the process of the experiment. In Figure 3, a core holder is used to hold the test core, and the gripper confining pressure is controlled by a hand pump. A pressure sensor for recording the different pressure at the inlet and outlet of the core is connected to both ends of the holder. The end of the device is connected to a cylinder for collecting the produced fluid in the course of experiment. The detailed descriptions about the experiment devices are as follows:

Pump: a high-pressure displacement pump is made in United States Chandler company. The pumping flow rate ranges from 0.01 μL/min to 50 mL/min (the pressure is not higher than 68 MPa), and the flow rate accuracy is ±0.3% (maximum seal leakage of 0.25 μL/min). Flow rate resolution is 0.01 μL/min, and it can reach up to 1.0 μL/min in constant pressure mode. The working pressure of the pump is 0.068 MPa~68 MPa, the pressure precision is ±0.5% under the constant temperature condition, and the pressure display resolution is 6.895 kPa.

Core holder: the core holder is Hastelloy triaxial core holder, which can effectively simulate the stress state of the core under formation conditions. The gripper was tested at 100 MPa for 4 hours without any leakage. The working pressure was 70 MPa, and the working temperature was 5°C~150°C.

Pressure sensor: the pressure sensor used for the experiment is DXD Series-Precision Digital Pressure Transducer. The test accuracy is ±0.02% and ±0.04% under the conditions 10°C~30°C and 30°C~50°C, respectively. The pressure resolution is 1 psi.

2.1. Experimental Core Samples. The experimental core samples are shown in Table 1. The sandstone core samples used

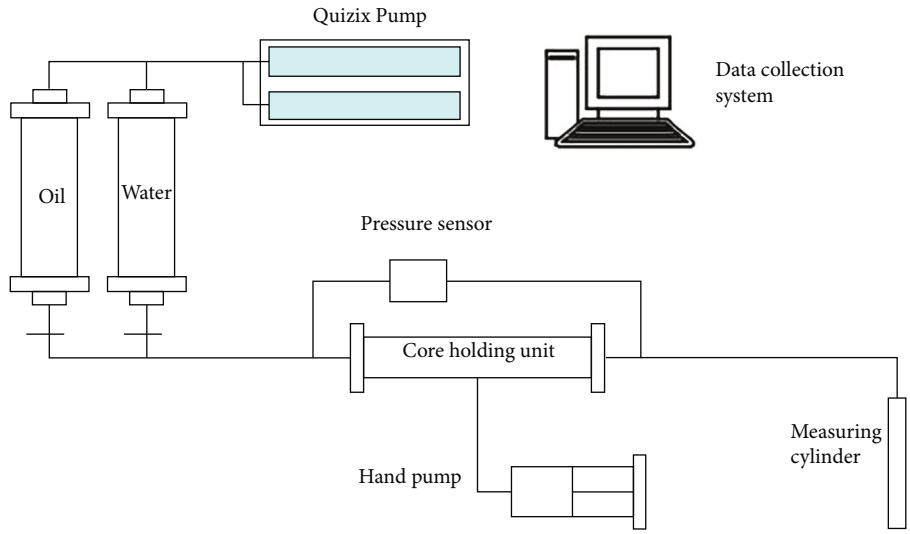

Figure 2: Schematic diagram of two-phase displacement experimental device.

Figure 3: Schematic diagram of main experimental equipment.

in this experiment are drilling cores from Heshui area in Ordos basin. The gas permeability of the core samples before hydraulic fracturing treatment is less than 0.3 mD, and the porosity ranges from 9.01% to 10.34%. It can be obviously observed that both the permeability and porosity are enhanced significantly after the construction of artificial fractures, especially the permeability in the study. The core samples are hydrophilicity.

3. Experiment Methods and Processes

The water displacement tests were carried out through unsteady method. The unsteady method is based on the Buckley-Leverett one-dimensional oil-water front advancement theory [31]. The unsteady-state method and steady-state method have main differences in the fluid injection and fluid distribution. The steady-state method simultaneously injects two fluids into the core, where the distribution of saturation in the porous medium is independent on distance and time. In terms of the unsteady-state method, the test core is saturated with a fluid first, then another fluid is injected into the core, and as a result, the saturation distribution is the function of oil and water movement distance and time.

In our experiment, the true-axial stress equipment is used to form a simple fracture, e.g., single fracture in the core sample. In the process of displacement, the fracture direction is approximately paralleled to the flow direction.

The selection of the injection rate and displacement pressure should satisfy the following relationship to reduce the influence of ending effect on the relative permeability of oil and water.

(i) Constant speed method: determining the water injection speed by the following equation:

$$L \times \mu_w \times v_w \geq 1, \tag{1}$$

where L is the rock sample length (cm), μ_w is the viscosity of water at the measured temperature, and v_w is the percolation velocity (cm/min)

(ii) Constant pressure method: determining the displacement pressure difference π_1 as follows:

$$\pi_1 = \frac{10^{-3}\sigma_{ow}}{\Delta p_o \sqrt{K_a/\phi}}, \tag{2}$$

where π_1 is the ratio of capillary pressure to displacement pressure, σ_{ow} is the oil-water interfacial tension (mN/m), Δp_o is the displacement pressure difference (MPa), K_a is the core permeability (D), and ϕ is the core porosity (%).

In this study, the experiments were carried out with the constant pressure method. The experiment procedures before the hydraulic fracturing treatment are as follows:

(i) After oil washing oil and drying, the core samples were weighed, then the cores were evacuated and saturated with brine, and the saturated cores were weighed again to obtain the effective pore volume

Table 1: Parameters of samples used in waterflooding tests.

Core	Length (cm)	Diameter (cm)	Permeability before hydraulic fracturing treatment (mD)	Permeability after hydraulic fracturing treatment (mD)	Porosity before hydraulic fracturing treatment (%)	Porosity after hydraulic fracturing treatment (%)
H1-5	4.25	2.52	0.29	0.67	10.34	10.44
H11	4.56	2.48	0.19	0.84	9.03	9.14
H13	4.30	2.54	0.12	0.95	9.012	9.20
H2-12	4.35	2.50	0.23	0.95	9.76	9.89

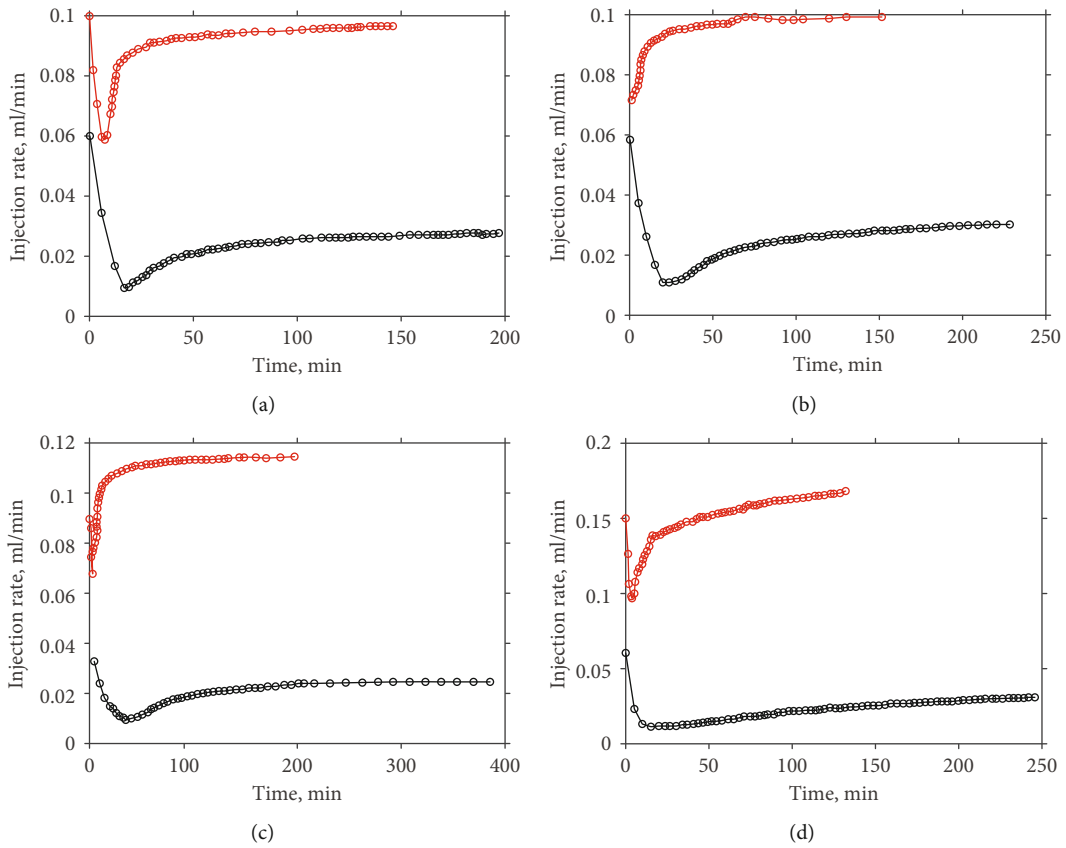

Figure 4: Injection velocity profile with respect to the waterflooding time before and after the construction of fracture in the experimental core. The red and black points represent the results before and after the construction of fracture. (a) Cores H1-5. (b) Cores H11. (c) Cores H13. (d) Cores H2-12.

(ii) Irreducible water saturation was formed by oil flooding. To fully establish the irreducible water saturation, the oil flooding speed should gradually increase from low to high, until no much more water is driven out. By measuring the volume of water driven by the oil, the irreducible water saturation was obtained

(iii) After oil displacement volume is up to 10 times of the pore volume, the effective permeability of the oil phase under irreducible water was measured three times consecutively with relative error less than 3%

(iv) The water displacement experiment was carried out to determine the appropriate displacement pressure according to the experimental design. The water breakthrough time, cumulative oil production, cumulative liquid production, displacement velocity, and displacement pressure differences between the two sides of rock specimen were recorded

(v) At the early stage of water breakthrough, the amount of oil at the specific time interval was recorded. Then, we should gradually lengthen the time interval with the decreasing of oil output.

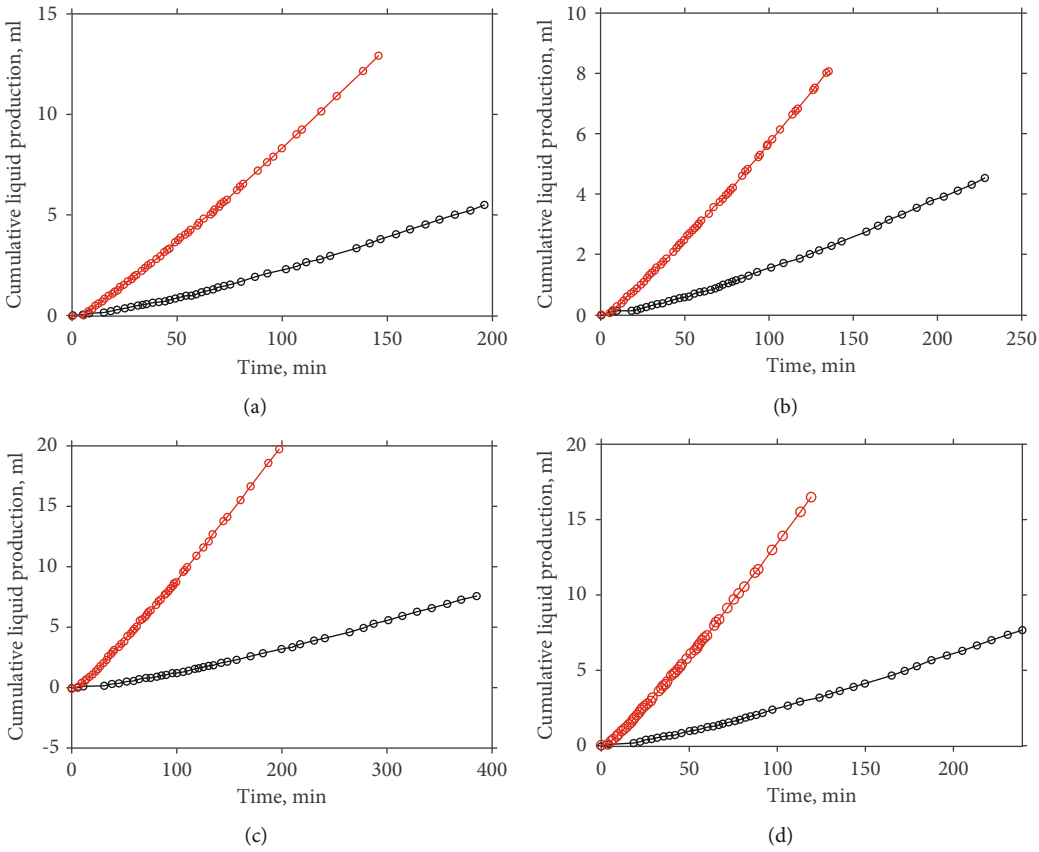

Figure 5: Cumulative liquid production with respect to the waterflooding tome before and after the construction of fracture in the experimental core. The red and black points represent the results before and after the construction of fracture. (a) Cores H1-5. (b) Cores H11. (c) Cores H13. (d) Cores H2-12.

When the water content reached 99%, the relative permeability of water phase under the residual oil situation was measured.

After the experiment, the core samples were washed by formaldehyde and toluene mixture, and then the core samples after the hydraulic fracturing treatment were performed. To reduce the influence of flooding conditions on the experimental results, the displacement experiments were carried out by the constant pressure method in the process of irreducible water and oil displacement.

The relationship between relative permeability and water saturation of unsteady oil and water is calculated according to the following equations:

$$f_o(S_w) = \frac{d\bar{V}_o(t)}{d\bar{V}(t)}, \tag{3}$$

$$K_{ro} = f_o(S_w)\frac{d\left[1/\bar{V}(t)\right]}{d\left\{I \times \bar{V}(t)\right\}}, \tag{4}$$

$$K_{rw} = K_{ro} \times \frac{\mu_w}{\mu_o} \times \frac{1 - f_o(S_w)}{f_o(S_w)}, \tag{5}$$

$$I = \frac{Q(t)}{Q_o} \times \frac{\Delta p_o}{\Delta p(t)} \tag{6}$$

$$S_w = S_{wc} + \bar{V}_o(t) - \bar{V}(t) \times f_o(S_w), \tag{7}$$

where $f_o(S_w)$ is the oil content, expressed in decimals, $\bar{V}_o(t)$ is the dimensionless cumulative oil production (fraction), $\bar{V}(t)$ is the dimensionless cumulative liquid production volume (fraction), K_{ro} is the oil relative permeability (decimals), K_{rw} is the relative permeability of the water phase (decimals), I is the relative injection capacity, also known as the flow capacity ratio, Q_o is the oil flow rate of the rock sample outlet at the initial moment (cm^3/s), $Q(t)$ is the volume of liquid produced at the outlet of the rock sample at time t (cm^3/s), Δp_o is the displacement pressure difference at the initial moment (MPa), $\Delta p(t)$ is the displacement pressure difference at time t (MPa), S_{wc} is the irreducible water saturation, and S_w is the water saturation.

4. Experiment Results and Analysis

4.1. Injection Speed. Figure 4 shows the injection velocity profile with respect to the waterflooding time before and after the construction of fracture in the experimental cores. Under the condition of constant pressure displacement, the injection velocity decreases continuously and

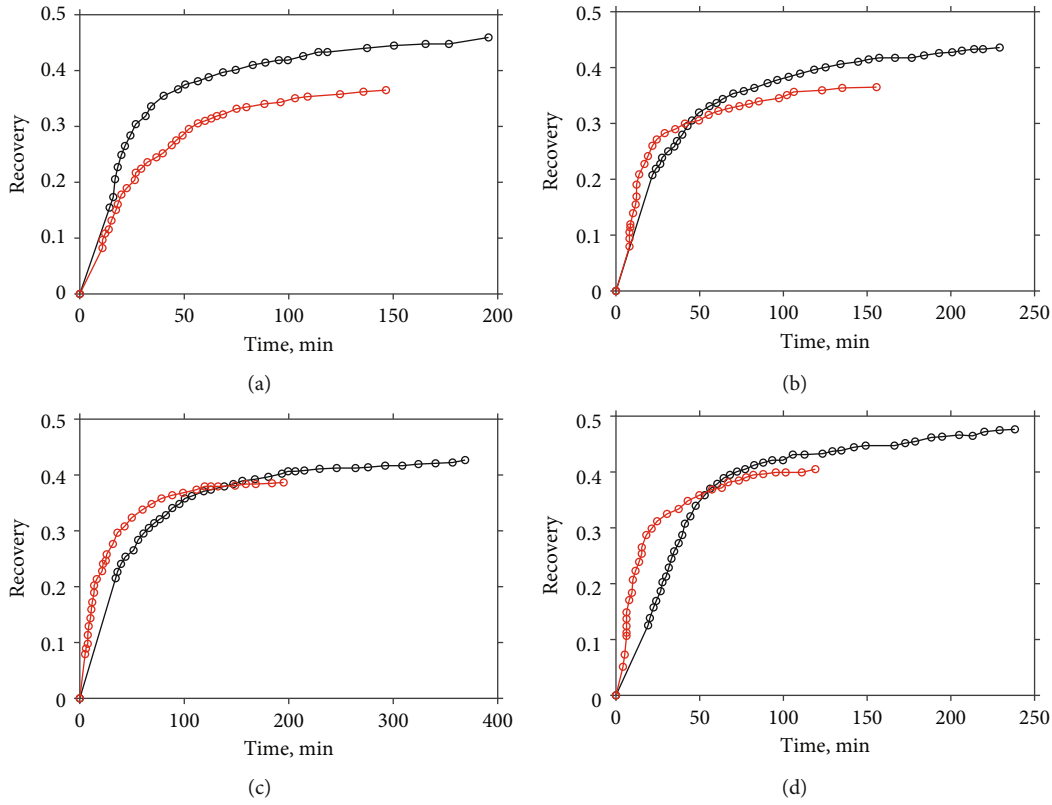

Figure 6: Oil recovery with respect to waterflooding time before and after the construction of fracture in the experimental core. The red and black points represent the results before and after the construction of fracture. (a) Cores H1-5. (b) Cores H11. (c) Cores H13. (d) Cores H2-12.

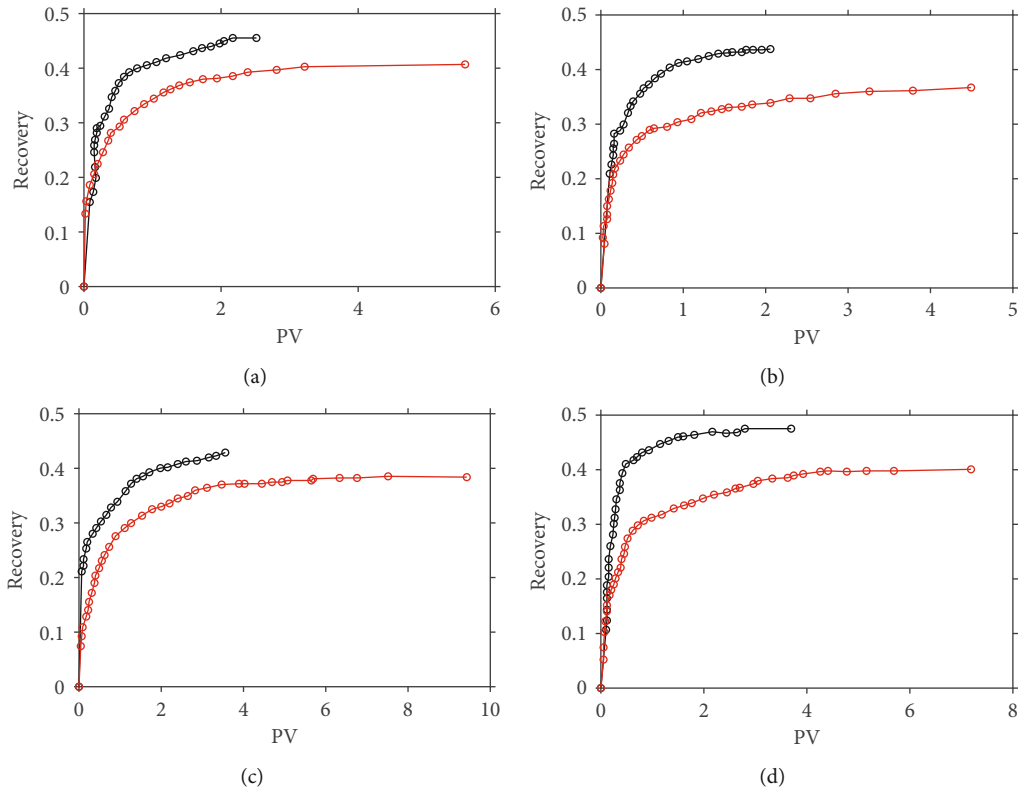

Figure 7: Oil recovery with respect to the injection volume before and after the construction of fracture in the experimental core. The red and black points represent the results before and after the construction of fracture. (a) Cores H1-5. (b) Cores H11. (c) Cores H13. (d) Cores H2-12.

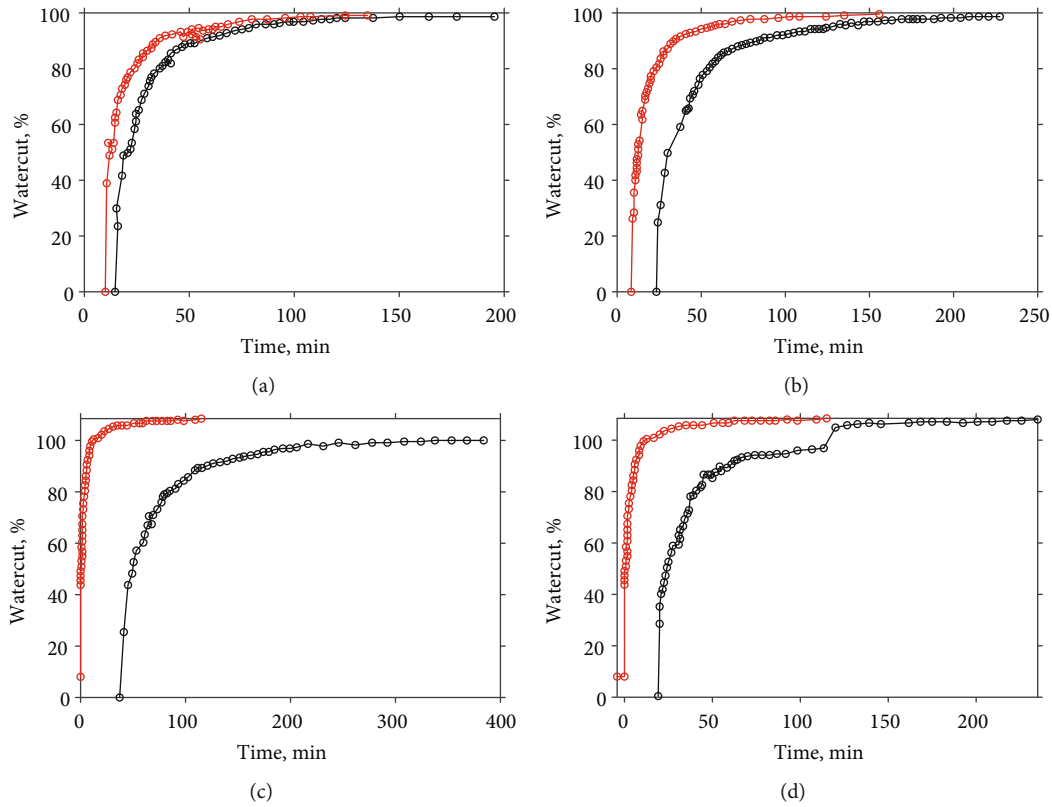

Figure 8: Water content with respect to the waterflooding time before and after the construction of fracture in the experimental core. The red and black points represent the results before and after the construction of fracture. (a) Cores H1-5. (b) Cores H11. (c) Cores H13. (d) Cores H2-12.

then rises continuously when the injection velocity drops to a certain value. In the process of oil-water displacement experiment, the resistance of the displacement phase at a certain location decreases with the increasing of saturation of the flooding phase. Therefore, under constant pressure displacement condition, the velocity in the core decreases before the water breakthrough. When the displacement front crosses the end, the core will form water breakthrough. As the oil phase is continuously driven out, the flow path increases, and the water flow resistance decreases. With constant pressure displacement, the injection rate increases continuously.

4.2. Cumulative Liquid Production. Figure 5 displays the cumulative liquid production versus time before and after the construction of fracture in the experimental core. At the same water displacement time, the cumulative fluid production of the cores with fractures was significantly higher than that without fractures. Due to the existence of fractures, the seepage resistance is highly reduced; as a result, the accumulated liquid production obviously increased, indicating that the water absorption capacity of the core is enhanced. However, it is worth noting that if the increment of fluid production per unit time in the core is too high, the water-bearing will increase rapidly.

4.3. Oil Recovery. Figure 6 shows the evolution of oil recovery with respect to waterflooding time before and after the construction of fracture in the experimental core. As the displacement time increases, the oil phase in the core is continuously driven out, and the oil recovery increases. The oil phase is a continuous phase in the early stage of displacement. Since the oil phase is distributed in the medium and large pores, the oil is easily driven out by the water phase with the help of capillary pressure. With the progress of the displacement process, the oil phase is divided into discontinuous phases due to the coupling influence of the Jarmine effect and blocking effect. The difficulty of displacement increases, and the movable oil in the core decreases; as a result, the increasing of the recovery rate becomes weak. It can be seen that the oil recovery increases after the construction of the fractures. The main reason is that the fractures improve the connectivity among the pores and reduce the seepage resistance; as a result, the oil phase is rapidly expelled by the aqueous phase. However, with the progress of displacement, the increasing rate of oil recovery decreases rapidly. At the end of the experiment, the ultimate recovery was lower than that of the core without fractures.

Although the fractures improve the connectivity among the pores and reduce the seepage resistance, the matrix permeability is still very low. The existence of high-permeable fractures enhances the heterogeneity of the core permeability which leads to a reduction of the displacement efficiency. We should note that the recovery factor is related to the microdisplacement efficiency and the macrosweep efficiency. In the actual production process, although the microdisplacement efficiency after

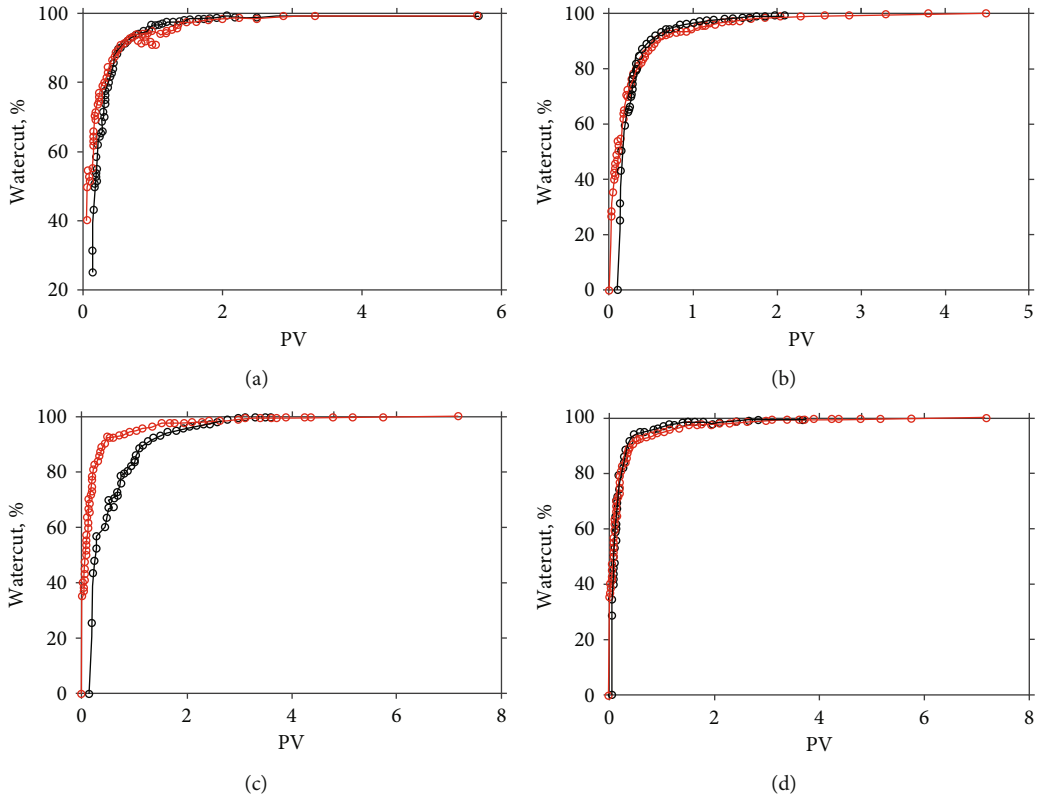

Figure 9: Relationship between water content and injection pore volume before and after the construction of fracture in the experimental core. The red and black points represent the results before and after the construction of fracture. (a) Cores H1-5. (b) Cores H11. (c) Cores H13. (d) Cores H2-12.

Table 2: Displacement indices of water-free displacement before and after the construction of fractures.

Rock samples	Type of experiment	Flooding characteristics at water-free displacement period			
		Injection time (min)	Production rate (mL/min)	Recovery ratio (%)	Injection volume
H1-5	Before fractured	12.23	0.0183	15.61	0.100
	After fractured	6.02	0.0195	8.08	0.053
H11	Before fractured	22.65	0.0103	18.62	0.111
	After fractured	8.00	0.0133	8.25	0.051
H13	Before fractured	36.34	0.0062	20.86	0.115
	After fractured	6.72	0.0139	7.98	0.047
H2-12	Before fractured	18.25	0.0081	12.85	0.070
	After fractured	4.05	0.0178	5.46	0.031

fracturing reduces, the macrosweep efficiency increases. Therefore, hydraulic fracturing technology can improve oil recovery.

Figure 7 shows the characteristics of the oil recovery with respect to the injection volume before and after the construction of fracture in the experimental core. As the injection volume increases, the number of pores in the water phase increases and therefore improves the oil recovery factor. As the displacement progresses, the number of pores that can be reached by the water phase is reduced. Therefore, the increasing rate of oil recovery gradually reduces.

The oil recovery rate of the core is lower than that without fractures. Before the formation of fractures, the advance of water phase is slow. Due to the existence of capillary pressure, the water phase can enter into the small pores, and therefore, the displacement is relatively full. After the high-permeable fractures form, the water rapidly advances along the high-permeable channels, and the oil phase is easily trapped inside the middle and small pores, which causes the reduction of displacement efficiency. We should point out that the capillary number increases due to the existence of fractures, and the trapped oil can be gradually driven out by the water phase.

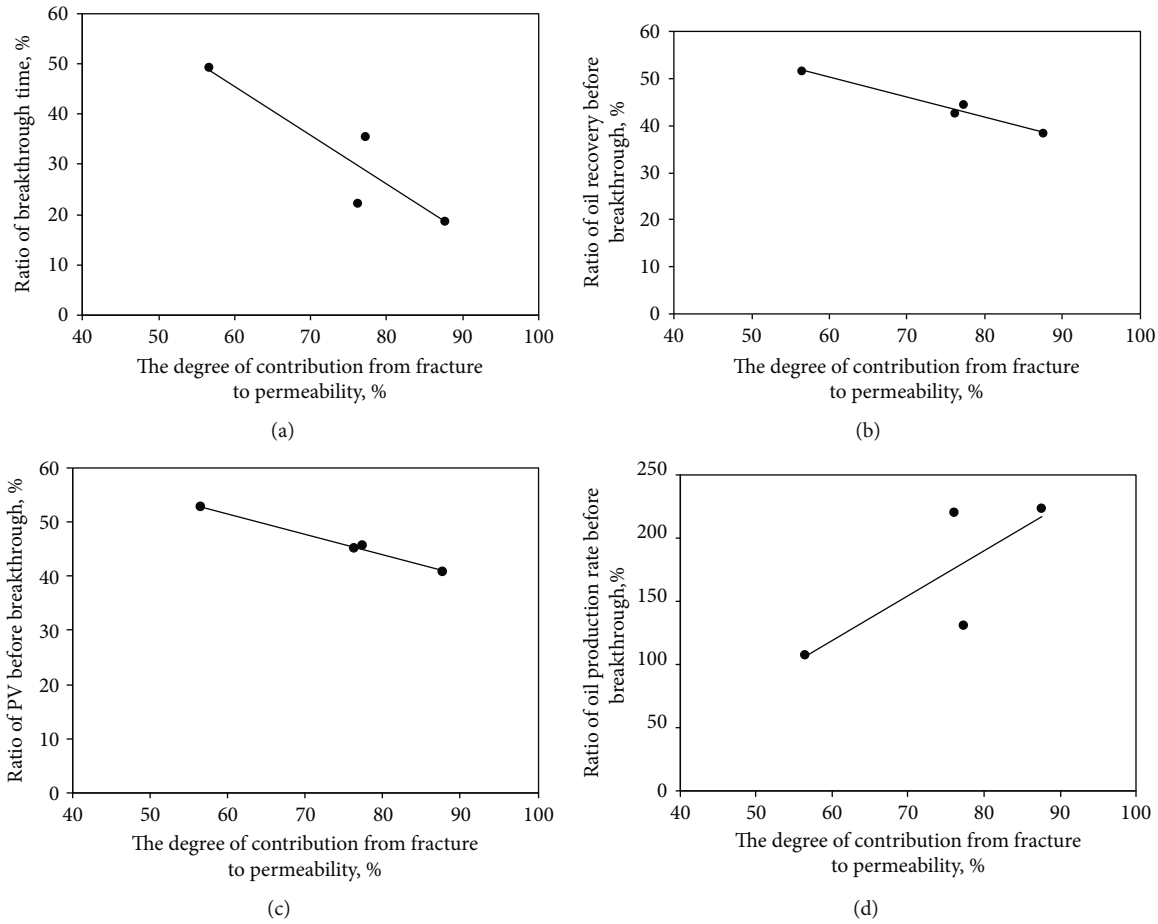

Figure 10: Contribution of fracture to permeability and the indices of displacement in water-free production stage. (a) Ratio of breakthrough times. (b) Oil recovery. (c) PV. (d) Oil production rate.

Table 3: Displacement index under different displacing periods.

Rock samples	Type of experiment	Water content is 95%		Water content is 98%		Final period	
		Recovery ratio (%)	Injection volume	Recovery ratio (%)	Injection volume	Recovery ratio (%)	Injection volume
H1-5	Before fractured	41.39	0.90	43.76	1.47	45.60	2.50
	After fractured	31.53	1.12	34.41	1.90	36.69	5.66
H11	Before fractured	39.71	0.82	42.11	1.33	43.69	2.08
	After fractured	30.77	1.00	34.67	2.56	36.84	4.49
H13	Before fractured	38.46	1.77	40.76	2.37	42.72	3.59
	After fractured	31.76	1.88	35.90	3.46	38.63	9.72
H2-12	Before fractured	42.06	0.69	45.26	1.47	47.58	3.64
	After fractured	32.62	1.33	37.28	2.62	40.29	7.17

4.4. Moisture Content. Figure 8 depicts the evolution of water content with respect to the waterflooding time before and after the construction of fracture in the experimental core. It can be clearly seen that the flow velocity is low before the hydraulic fracturing treatment. The moisture content at the outlet of the core increases slowly as the displacement time. After forming the fractures, the fractures will form high-permeable channels, where water can quickly move forward. The water is rapidly driven out at the core outlet, and water content increases rapidly after breakthrough.

Figure 9 shows the relationship between the water content and the injection pore volume. In the early stage of displacement, under the same injection volume condition, the water content at the outlet of the core is higher than that without fractures. It reveals that the displacement efficiency of the core with the fractures is relatively low, which is consistent with the previous analysis.

Table 4: Increment of recovery and PV under different displacing periods.

Rock samples	Type of experiment	When water content is 95% to 98%			When water content is 98% to the final		
		Recovery increment	Injection multiple increment	Recovery/ PV	Recovery increment	Injection multiple increment	Recovery/ PV
H1-5	Before fractured	2.37	0.57	4.20	1.84	1.03	1.79
	After fractured	2.88	0.78	3.67	2.27	3.76	0.60
H11	Before fractured	2.40	0.51	4.70	1.58	0.75	2.10
	After fractured	3.90	1.56	2.51	2.17	1.93	1.13
H13	Before fractured	2.29	0.60	3.84	1.96	1.22	1.61
	After fractured	4.14	1.58	2.62	2.73	6.26	0.44
H2-12	Before fractured	3.20	0.78	4.10	2.32	2.17	1.07
	After fractured	4.66	1.29	3.61	3.02	4.56	0.66

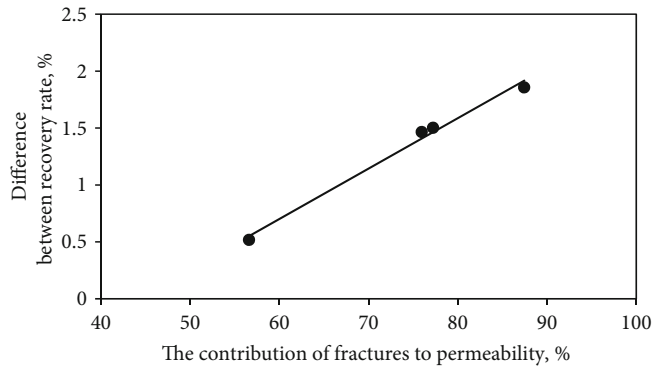

Figure 11: Differential recovery of prefractured and fractured cores where water cut rises from 95% to 98%.

When water content is about 80%-90%, the moisture content curves for the cores with and without fractures intersect. As the injection rate increases, the water content at the end of the core increases slowly. The main reason stems from the difference of the core injection ability with and without fractures. Before the fracture is formed, the moisture content is 80%-90%, which belongs to middle and late stage of displacement. The injection capacity is low, which results in a limited ability to displace oil phase. Therefore, the moisture content of the core increases rapidly. By contrast, after the fracture is formed, the moisture content 80%-90% belongs to the predisplacement stage. The presence of fractures improves the core injection capacity. The water phase continuously flows along the high-permeable channels and therefore increases the oil displacement efficiency.

5. Discussions

To further analyze the displacement characteristics of the core with and without the fractures, the waterflooding indices at different displacement stages are presented. Table 2 shows the indices of water-free displacement before and after the construction of the fracture.

Due to the existence of fractures, the pore connectivity enhances while the seepage resistance decreases. It significantly shortens the water-free displacement period. As the existence of fractures enhances the permeability heterogeneity, the number of pores that can be swept by the displacement front is reduced, leading to a significant reduction of oil recovery. The injection capacity increases as the existence of fractures. The average oil recovery rate at the water-free displacement period obviously increases, and the required injection times decrease correspondingly. As a result, it can be concluded that the presence of fractures can effectively enhance the oil production rate.

Figure 10 plots the contribution of fracture to permeability and the indices of displacement in water-free production stage. It can clearly be seen that the greater the contribution of the fracture to the permeability, the earlier the core drives out water. The lower the seepage resistance after the fractures are formed, the faster the displacement speed of the flooding front, therefore, the higher the average oil production rate at the water-free production stage. The difference of matrix permeability and fracture permeability is generally quit large. The greater the contribution of fractures to core permeability, the stronger the heterogeneity of core permeability due the presence of fractures.

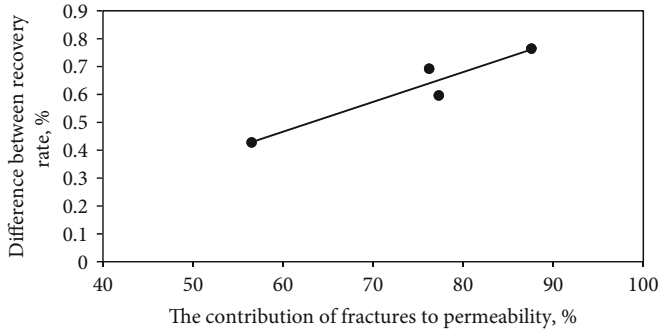

Figure 12: Differential recovery of prefractured and fractured cores where water cut rises from 98% to 99.95%.

The results related to the displacement indices under different displacement periods are presented in Table 3. When the fractured core is saturated with water content of 95% and 98%, the ultimate recovery ratio is lower than that without fractures, and the injection time increases as well in the corresponding period. As we have mentioned above, the presence of fractures reduces the flow resistance and therefore results in a lower displacement efficiency.

As shown in Table 4, increasing the water content from 95% to 98% and from 98% to 99.95% (the end of the experiment), respectively, the enhanced oil recovery per unit volume of injection water decreases, indicating that the microdisplacement efficiency of the cores reduces due to the presence of fractures. However, the increase in core recovery after hydraulic fracturing treatment is higher than that before fracturing. The erosion of the high-velocity water along the high-permeability channels leads to an increase of the core recovery at the late stage of displacement. The high-velocity water erosion increases the capillary number and thus allows the water phase easily to enter into the relatively small pores. Due to the existence of fractures, the oil recovery ratio can improve as the injection rate and displacement velocity increase at the late stage of displacement. Figures 11 and 12 show the relationship between the recovery difference and the contribution of fracture to permeability, respectively. As the contribution of the fracture to the permeability increases, the core recovery after fracturing increases.

6. Conclusions

In this study, the unsteady-state displacement method was used to investigate the characteristics of oil-water two-phase displacement with and without fractures in tight sandstone core. Since the fractures in the tight sandstone reservoir provide the high-permeable channels, the seepage resistance decreases dramatically at the presence of fractures, which further results in the changes of the water injection speed, cumulative production, recovery ratio, and water content accordingly. Based on the experimental results, some conclusions are summarized as follows:

(i) The presence of fractures increases the injection velocity under the same displacement pressure. Before the water breakthrough, the decreasing rate of injection rate becomes small, while after the water breakthrough occurs, the rapid reduction of seepage resistance results in an improvement of injection rate

(ii) Due to the presence of fractures, the accumulated fluid production of the core obviously improves

(iii) The heterogeneity of core permeability is enhanced at the presence of fractures, which improves the increasing rate of core recovery at the early displacement stage. As the displacement progresses, the core recovery rapidly decreases. As the injection volume increases, the recovery factor increases. The number of pores that can be reached by the aqueous phase reduces

(iv) After water breakthrough, the water content increases rapidly at the presence of fractures. In the early stage of displacement, the water content at the outlet improves. The displacement efficiency of the core is relatively low after the hydraulic fracturing treatment. In the middle and high water cut stage, with the increase of the injection volume, the water content of the core outlet increases relatively slowly at the presence of fractures

(v) Before water breakthrough, the core injection time significantly decreases, and the water cut period significantly shortens. The recovery rate obviously reduces, while the water absorption capacity of the core increases. At the water-free production stage, the average oil production rate increases significantly, and the required injection time decreases significantly. The greater the contribution of fractures to permeability, the earlier the water breakthrough occurs.

Data Availability

The experimental data used to support the findings of this study are available from the corresponding author upon request.

Conflicts of Interest

The authors declare that there is no conflict of interest regarding the publication of this article.

Acknowledgments

This work is supported by the Science Foundation of China University of Petroleum, Beijing (No. 2462021BJRC005), NNSF of China (No. U1562102), and the Important National Science & Technology Specific Projects (No. 2016ZX05047005-001).

References

[1] Y. Liu, B. M. Yu, and B. Xiao, "A fractal model for relative permeability of unsaturated porous media with capillary pressure effect," *Fractals*, vol. 15, no. 3, pp. 217–222, 2007.

[2] J. C. Noirot, P. J. van den Hoek, D. Zwarts et al., "Water injection and water flooding under fracturing conditions," in *Paper SPE 81462, Presented at the SPE 13th Middle East Oil Show & Conference*, Bahrain, April 5-8, 2003.

[3] J. Li, X. Song, C. Tian et al., "Single sandbody stacking pattern, calcareous barrier and fracture of tight low permeability oil sandstone reservoir and their impact on water-flooding - a case study of Ansai oil field, Ordos Basin, China," in *Paper SPE 175605, Presented at the SPE Reservoir Characterisation and Simulation Conference*, Abu Dhabi, UAE, September 14-16, 2015.

[4] M. J. Mayerhofer, E. P. Lolon, N. R. Warpinski, C. L. L. Cipolla, D. Walser, and C. M. M. Rightmire, "What is stimulated reservoir volume?," *SPE Production & Operations*, vol. 25, no. 1, pp. 89–98, 2010.

[5] J. H. Li, X. M. Song, T. Yu, J. Hou, and Z. Lei, "Dynamic fractures in tight low-permeability oil sandstone reservoirs," in *Paper SPE 185992, Presented at the SPE Reservoir Characterisation and Simulation Conference*, Abu Dhabi, UAE, May 9-10, 2017.

[6] L. Tian, D. Y. Yang, S. X. Zheng, and B. Feng, "Parametric optimization of vector well patterns for hydraulically fractured horizontal wells in tight sandstone reservoirs," *Journal of Petroleum Science and Engineering*, vol. 162, pp. 469–479, 2018.

[7] A. Moinfar, A. Varawei, K. Sepehrnoori, and R. T. Johns, "Development of a coupled dual continuum and discrete fracture model for the simulation of unconventional reservoirs," *Paper SPE 163647, Presented at the SPE Reservoir Simulation Symposium Held in the Woodlands*, 2013, Texas USA, February 18-20, 2013, 2013.

[8] J. E. Warren and P. J. Root, "The behavior of naturally fractured reservoirs," *SPE Journal*, vol. 3, no. 3, pp. 245–255, 1963.

[9] H. Kazemi, "Pressure transient Analysis of naturally fractured reservoirs with uniform fracture distribution," *SPE Journal*, vol. 9, no. 4, pp. 451–462, 1969.

[10] O. A. De Swaan, "Analytical solution for determining naturally fractured reservoir properties by well testing," *SPE Journal*, vol. 16, pp. 117–122, 1976.

[11] B. M. Yu, "Fractal character for tortuous streamtubes in porous media," *Chinese Physics Letters*, vol. 22, no. 1, pp. 158–160, 2005.

[12] A. Moinfar, A. Varavei, K. Sepehrnoori, and R. T. Johns, "Development of an efficient embedded discrete fracture model for 3D compositional reservoir simulation in fractured reservoirs," *SPE Journal*, vol. 19, no. 2, pp. 289–303, 2014.

[13] M. Ţene, S. Bosma, M. S. al Kobaisi, and H. Hajibeygi, "Projection-based embedded discrete fracture model (pEDFM)," *Advances in Water Resources*, vol. 105, pp. 205–216, 2017.

[14] B. M. Yu and J. H. Li, "Some fractal characters of porous media," *Fractals*, vol. 9, no. 3, pp. 365–372, 2001.

[15] J. Chang and Y. C. Yortsos, "Pressure transient analysis of fractal reservoirs," *SPE Formation Evaluation*, vol. 5, no. 1, pp. 31–38, 1990.

[16] M. Sahimi, "Flow phenomena in rocks: from continuum models to fractals, percolation, cellular automata, and simulated annealing," *Reviews of Modern Physics*, vol. 65, no. 4, pp. 1393–1534, 1993.

[17] L. Guarracino, "A fractal constitutive model for unsaturated flow in fractured hard rocks," *Journal of Hydrology*, vol. 324, no. 1–4, pp. 154–162, 2006.

[18] K. Zhang, N. Jia, F. Zeng, and P. Luo, "A new diminishing Interface method for determining the minimum miscibility pressures of light oil–CO2 systems in bulk phase and nanopores," *Energy & Fuels*, vol. 31, no. 11, pp. 12021–12034, 2017.

[19] K. Zhang and Y. Gu, "Two new quantitative technical criteria for determining the minimum miscibility pressures (MMPs) from the vanishing interfacial tension (VIT) technique," *Fuel*, vol. 184, no. 11, article 136144, pp. 136–144, 2016.

[20] P. Lian, L. Cheng, and L. Liu, "The relative permeability curve of fractured carbonate reservoirs," *Acta Petrolei Sinica*, vol. 32, no. 6, pp. 1026–1030, 2011.

[21] T. C. Rasmussen, "Laboratory characterization of fluid flow parameters in a porous rock containing a discrete fracture," *Geophysical Research Letters*, vol. 22, no. 11, pp. 1401–1404, 1995.

[22] E. Joonaki and S. Ghanaatian, "Prediction of relative permeability for multiphase flow in fractured oil reservoirs by using a soft computing approach," *International Journal of Computer Applications*, vol. 73, no. 16, 2013.

[23] M. C. Leverett, "Flow of oil-water mixtures through uconsolidated sands," *Transactions of the AIME*, vol. 132, no. 1, pp. 149–171, 1939.

[24] L. A. Rapoport and W. J. Leas, "Properties of linear waterfloods," *Journal of Petroleum Technology*, vol. 5, no. 5, pp. 139–148, 1953.

[25] T. Maldal, A. Gulbrandsen, and E. Gilje, "Correlation of capillary number curves and remaining oil saturations for reservoir and model sandstones," *In Situ*, vol. 21, pp. 239–270, 1997.

[26] S. E. Buckley and M. C. Leverett, "Mechanism of fluid displacement in sands," *Transactions of the AIME*, vol. 146, no. 1, pp. 107–116, 1942.

[27] H. J. Welge, "A simplified method for computing oil recovery by gas or water drive," *Journal of Petroleum Technology*, vol. 4, no. 4, pp. 91–98, 1952.

[28] J. M. Schembre and A. R. Kovscek, "A technique for measuring two-phase relative permeability in porous media via X-ray CT measurements," *Journal of Petroleum Science and Engineering*, vol. 39, no. 1-2, pp. 159–174, 2003.

[29] S. Bryant and M. Blunt, "Prediction of relative permeability in simple porous media," *Physical Review A*, vol. 46, no. 4, pp. 2004–2011, 1992.

[30] Z. Lianbo and L. Xiang-Yang, "Fractures in sandstone reservoirs with ultra-low permeability: a case study of the Upper Triassic Yanchang Formation in the Ordos Basin, China," *AAPG Bulletin*, vol. 93, no. 4, pp. 461–477, 2009.

[31] K. Spayd and M. Shearer, "The Buckley-Leverett equation with dynamic capillary pressure," *SIAM Journal on Applied Mathematics*, vol. 71, no. 4, pp. 1088–1108, 2011.